Time-Dependent Microwave Radiometry for the Measurement of Temperature in Medical Applications

Fernando Bardati, Gaetano Marrocco, *Member, IEEE*, and Piero Tognolatti, *Member, IEEE*

***Abstract*—Microwave radiometry has been considered for the noninvasive monitoring of internal temperature in biological bodies when the temperature is varied under the control of external sources and contacting fluid. The body temperature is modeled as a discrete-time controlled statistical process, whose estimate is cyclically updated exploiting radiometric measurements. The Kalman filter has been used, which is able, with the proper choice of parameters, to balance the temperature retrieval between *a priori* information and measurements. Prospective applications to medicine have been investigated for temperature monitoring within a neonatal head during a hypothermia treatment.**

***Index Terms*—Biomedical measurement, hypothermia, Kalman filter, microwave radiometry.**

I. Introduction

MICROWAVE radiometry is well assessed as a monitoring tool in remote-sensing geophysical applications with a nondense medium often sensed by a remote antenna [1]. Over the last 25 years, it has also been proposed as a noninvasive, possibly noncontacting, technique for temperature measurements within nonaccessible dense bodies in view of medical and other applications, where instead, the antenna is close to or contacts the body, so that the antenna near-field is generally involved in sensing [2]–[11]. Prospected applications to medicine include concurrent temperature monitoring during hyperthermia heating in oncology and therapeutic hypothermia, and passive diagnosis of inflammation states, typically malignancies, as an alternative to assessed bio-imaging techniques. In the last application, the heating of the body has been also considered as an expedient to enhance the temperature differential between tumor and healthy tissue.

Microwave radiometry's effectiveness in determining the subsurface temperature basically relies on the weighting functions, whose extinction depth roughly is one-half the skin depth δ_s of the sensed material. At the highest frequencies, microwave radiometry does not provide more information than infrared radiometry, i.e., the body superficial temperature. However, even if we are only interested in the thermal structure of the δ_s layer at the lowest explored frequency, the main drawback of microwave radiometry is the scarce spatial resolution of a temperature retrieval. This is due to the low signal-to-noise ratio of radiometric data as are acquired with the usual integration times of a few seconds or less. As a consequence, two measurements performed at two close frequencies do not provide independent information on the temperature to be retrieved. Due also to the overall complexity of additional radiometric channels, only 2–5 frequencies are typically explored in multifrequency systems. This dramatically reduces spatial resolution.

To partially counteract the above drawbacks of microwave radiometry, the use of reliable and complementary *a priori* information has been proposed in such a way that the few degrees of freedom of microwave measurements can be successfully spent to estimate the temperature against noise [12]. In this paper, we assume that the temperature within a body is a result of known heat exchanges that can be described by mathematical-physics equations and that noise and other uncertainties can be statistically modeled. A discrete model in time and space has been arranged as a statistical process and complemented with noisy measurement equations, which are assumed cyclically performed by a multichannel radiometer. The Kalman filter has then been exploited for the retrieval of the thermal state. A numerical analysis has been performed to evaluate microwave radiometry supported by Kalman filtering in the estimation of nonsuperficial temperatures.

We considered the temperature estimate within a neonatal head during hypothermia. Hypothermia of a newborn-infant brain has been proposed as a neuroprotective therapy after hypoxia ischaemia [13]–[17]. Selective head cooling is considered to be a safe alternative for systemic hypothermia for the newborn infant. Preliminary results of selective head cooling indicate that moderate brain hypothermia may be applied to newborn infants while minimizing the deleterious effects of systemic hypothermia. Selective head cooling is accomplished by applying cool packs to the parieto-temporal regions or by circulating cold water through a coil of tubing wrapped around the head or other caps. The rectal, fontanelle, naso-pharyngeal, or tympanic temperatures were monitored during the experiments on infants, while temperature probes were inserted in the brain in the experiments on piglets, and their outcomes were correlated with the temperatures obtained at noninvasive monitoring points. There is an evident interest, however, in noninvasive tools, therefore, microwave radiometry has been proposed. This technique can benefit by the relatively small sizes of the newborn infant brain.

Manuscript received September 30, 2003; revised April 7, 2004.

F. Bardati and G. Marrocco are with the Dipartimento di Informatica, Sistemi e Produzione, Università degli Studi di Roma "Tor Vergata," 00133 Rome, Italy.

P. Tognolatti is with the Dipartimento di Ingegneria Elettrica, Università degli Studi dell' Aquila, 67040 L'Aquila, Italy (e-mail: tognolatti@ing.univaq.it).

Digital Object Identifier 10.1109/TMTT.2004.832003

0018-9480/04$20.00 © 2004 IEEE

II. Radiometric Equation

Microwave radiometry is the measurement of the electromagnetic power spontaneously emitted by a lossy body in the microwave frequency range. Charged particles in motion are primary sources of incoherent thermal emission. Thermal radiation propagates inside the body where it is partially absorbed and partially irradiated externally. A wide-band antenna system collects and transduces the radiation to an electrical current fluctuating in the receiver's input unit, whose first- and second-order moments are defined radiometric signal and noise, respectively. For later use, let τ (integration time) denote the time interval over which means are computed.

If we assume the body Ω in local thermodynamic equilibrium and stationary in its electrical properties, the spectral content of the radiometric signal can be related to the local temperature, allowing the retrieval of temperature to be attempted from radiometric data. As a consequence of the Rayleigh–Jeans approximation of Planck's law, it is indeed possible to introduce a linear dependence $T(\underline{r}', t)W(\underline{r}, \underline{r}', \delta B_p)dV'$, with W being weighting function, between an elemental volume dV' at position $\underline{r}' \in \Omega$ having a physical temperature T, and the power $K_B \delta B_p dT_{av}(\underline{r})$ exchanged over a band δB_p with the antenna located at $\underline{r} \notin \Omega$. K_B is the Boltzmann's constant. By integration over the body, the available temperature is obtained as

$$T_{av}(\underline{r}, \delta B_p) = \int_{\Omega} T(\underline{r}', t)W(\underline{r}, \underline{r}', \delta B_p)dV' \tag{1}$$

with the weighting function normalized according to

$$\int_{\Omega} W(\underline{r}, \underline{r}', \delta B_p)dV' = 1. \tag{2}$$

A calibration is usually performed to transform the signal provided by a radiometric device to the available temperature of the body. The frequency range over which measurements are performed lies between 500 MHz and a few gigahertz. This range is discretely spanned in a multifrequency system by radiometric channels having band $\delta B_p, p = 1, P$ for a system with P channels. The weighting function can be obtained as the electromagnetic power deposition at $\underline{r}'$ when the antenna radiates from $\underline{r}$ onto the body with the normalization in (2). W depends on the antenna, frequency, and dielectric properties of the body [18], [19]. Tissue permittivity ε and electrical conductivity σ_e are assumed independent of T to preserve the linearity of the inverse problem. Since they change by a few percents per one degree of change of temperature, a linear model is only acceptable for small variations of sensed temperatures.

III. Discrete-Time Model

The biophysical situation to be modeled is a segment Ω of the human body, the temperature of which is governed by external and internal agents and is measured by a radiometric system.

We assume that the balance of heat exchanges can be modeled by the Pennes bio-heat equation [20], [21]

$$\rho C \frac{\partial T}{\partial t} = \nabla \cdot (\kappa \nabla T) + M_0 - \rho_b C_b w(T - T_b) + Q_e \tag{3}$$

which holds in Ω with the local temperature T a continuous function of position $\underline{r}$ and time t. The thermal problem is specified by a radiation boundary condition on the boundary $\partial\Omega$ as

$$\kappa \nabla T \cdot \hat{n} + h(T - T_a) = 0. \tag{4}$$

The symbols have the following meaning: ρC is the heat capacity ($\rho_b C_b$ for blood), κ is the thermal conductivity, M_0 is the metabolic heat generation, w is the blood perfusion rate, T_b is the arterial blood temperature, $\hat{n}$ is outward normal to $\partial\Omega$, and h is the surface conductivity. Q_e is the power density delivered to the body by a source, while T_a is the temperature of the external medium (e.g., a fluid) contacting Ω at points $\underline{r}_S$ belonging to the boundary. The body may be composed with different tissues. We assume that ρ, C, κ, M_0, w, T_b, and h are constant for each tissue segment and that the temperature changes are quite small so that they are also independent of T and time. However, in order to model the heat exchange with a contacting fluid, which may change before a treatment and during it, we let h assume different constant values for $t < 0$ and $t > 0$. The continuity of temperature and heat flux $\kappa \nabla T \cdot \hat{n}$ at the interface S_{ab} with normal $\hat{n}$ between different media is formulated as

$$T^+ - T^- = 0 \quad \kappa^+ \nabla T^+ \cdot \hat{n} - \kappa^- \nabla T^- \cdot \hat{n} = 0 \tag{5}$$

with T^-, T^+ (κ^-, κ^+) being the temperature (thermal conductivity) of the two faces of S_{ab}.

We assume that control inputs Q_e and T_a govern the temperature $T(\underline{r}, t) = T_0(\underline{r}) + \vartheta(\underline{r}, t)$ for $t > 0$, with T_0 being a basal temperature for $t < 0$. For the sake of simplicity, we pose $Q_e(\underline{r}, t) = S(\underline{r})u_1(t)$ with $S(\underline{r})$ being the heating pattern of the source and $u_1(t)$ being its strength. Such a factorization is appropriate, e.g., for a hyperthermia applicator at a fixed position with respect to the treated volume. Similarly, the temperature T_a is a stationary ambient temperature T_{env} for $t < 0$, while $T_a = T_{env} + u_2(t)$, with $u_2(t)$ being a forcing term for $t > 0$. The equation is a simple model for the fluid temperature inside a cooling bag in contact with the body for $t > 0$ during a hypothermia session, with $u_2(t)$ being a negative step function of proper strength.

It should be observed that the blood temperature and metabolic heat generation terms can be considered additional independent control inputs in the Pennes' equation (3).

The next step is to transform (3) and (4) to algebraic equations [22]. An explicit forward-difference scheme can be used for time derivatives, while central-difference approximations are used for spatial derivatives. According to well-known procedures, the various functions are evaluated at nodal points. In the following, ϑ^n_{ijk} will denote $\vartheta(\underline{r}, t)$ computed at $t = n\delta t$, $x = i\delta$, $y = j\delta$, and $z = k\delta$, and similarly for other functions. After substitution, (3) yields (6), shown at the bottom of the following page, for $(i\delta, j\delta, k\delta) \in \Omega$ and a homogeneous tissue with parameters ρ, C, κ, and w. When the point i, j, and k belongs to $\partial\Omega$, the central difference scheme in (6) includes one or more nodal points outside Ω. Such unknowns are eliminated, resorting to the discrete version of the boundary equation

(4), e.g., for a boundary (locally) parallel to the yz-plane, with $\hat{n} = -\hat{x}$

$$\kappa \frac{\vartheta^{n-1}_{i+1,j,k} - \vartheta^{n-1}_{i-1,j,k}}{2\delta} = h\left(\vartheta^{n-1}_{i,j,k} - u_2^{n-1}\right). \tag{7}$$

Attention must be given to the case where the point lies on the interface between different homogeneous tissues. While the average is used for parameters such as ρ, C, and w of adjacent tissues, the operator $\nabla \cdot \kappa \nabla \vartheta$ is approximated, with conduction occurring only in the x-direction as

$$\frac{\kappa^- + \kappa^+}{\delta^2}\left(\frac{\kappa^+ \vartheta^{n-1}_{i+1,j,k} + \kappa^- \vartheta^{n-1}_{i-1,j,k}}{\kappa^+ + \kappa^-} - \vartheta^{n-1}_{i,j,k}\right) \tag{8}$$

where κ^- and κ^+ are thermal conductivities at points $i-1$, j, k and $i+1$, j, k, respectively. For the conduction terms in the y- and z-directions, expressions similar to the above equation have to be added and substituted into (6) instead of the central differences.

A system of linear equations is obtained, enforcing the above equations at nodal points. An application $(i,j,k) \rightarrow m, m = 1, M$ can be used to form a vector $\vartheta_n \in R^M$ with the mth component $(\vartheta_n)_m = \vartheta^n_{i,j,k}$. M is the total number of nodal points. The set of equations can be finally rearranged as a discrete-time controlled process as

$$\vartheta_n = A\vartheta_{n-1} + Bu_{n-1} \tag{9}$$

with A being an $M \times M$ matrix, u_n being a two-element control input $u_n \equiv (u_1(t_n), u_2(t_n))$, and B being a $M \times 2$ matrix. The matrix A relates the state at the previous time step $n-1$ to the state at the current step n in the absence of driving functions.

Equation (9) solves the transient problem with the initial condition $\vartheta_0 = 0$ for $t = 0$. The steady-state problem in T_0, having sources M_0 and $T_0 - T_b$ in Ω and $T_0 - T_{env}$ in $\partial\Omega$ generates, in the absence of noise, a constant radiometric signal that will not receive further consideration in this paper. Other numerical procedures have been proposed [23] to transform the bio-heat equation into the discrete-time process (9), however, a finite-difference scheme is adequate for the following numerical analysis. Since the solver is explicit, the time step has to be small to avoid instability, however, implicit solvers yield state equations in a more complicated form than that in (9). The condition for stability is

$$\frac{\delta t}{\rho C}\left(\frac{6\kappa}{\delta^2} + \rho_b C_b w\right) < 1 \tag{10}$$

for the upgrade of temperature at a nodal point inside a homogeneous tissue and is a little more complicated at boundary points.

IV. Solving the Inverse Problem by Kalman Filtering

Data can be obtained for different positions $\underline{r}_q$ of the antenna with respect to the body and for different radiometric bands δB_p. Assume that N measurements are performed at each time step during a treatment. An application $(p,q) \rightarrow \ell$, $\ell = 1, L$ can be used to form a vector $g_n \in R^L$, which accounts for the transient temperature contribution to the radiometric available temperature. From (1), the ℓth component of g_n is computed as

$$(g_n)_\ell = \int_\Omega \vartheta(\underline{r}', t_n) W(\underline{r}_q, \underline{r}', \delta B_p) dV'. \tag{11}$$

Since ϑ can be considered constant within a cube having the center in i, j, k, a discrete version of (1) is

$$g_n = H\vartheta_n + \nu_n \tag{12}$$

with H is an $L \times M$ matrix, relating measurements to a thermal state. A measurement noise vector ν_n has been added. For the sake of simplicity, we assume the noise to be mutually uncorrelated between different measurements, i.e., $(\nu_n)_\alpha$ and $(\nu_n)_\beta$ are statistically uncorrelated for any pair α and β. We also introduce the noise standard deviation vector $\widetilde{\sigma}$, whose ℓth component is given by

$$(\widetilde{\sigma})_\ell = \left\langle (\nu_n)^2_\ell \right\rangle^{\frac{1}{2}} \tag{13}$$

where $\langle\ \rangle$ denotes expectation.

The inverse problem is the retrieval of state ϑ_n from measurements g_n in the presence of noise. We shall deal with this problem resorting to Kalman filtering [24], [25], which addresses the general problem of trying to estimate the state ϑ of a discrete-time controlled process that is governed by the linear stochastic difference equation

$$\vartheta_n = A\vartheta_{n-1} + Bu_{n-1} + w_n. \tag{14}$$

The random variable w_n represents the state noise. Indeed, we assume that different state realizations, i.e., temperature distributions, may exist for identical initial conditions and control inputs. ν_n and w_n are assumed to be independent of each other, with zero means and covariance matrices R and Q, respectively. Let $\hat{\vartheta}^-_n$ be the *a priori* state estimate at step n, and $\hat{\vartheta}_n$ be the *a posteriori* state estimate at step n given measurement g_n. The Kalman filter computes the *a posteriori* state estimate as a linear combination of the *a priori* estimate and a weighted difference between the actual measurement g_n and the predicted measurement $H\hat{\vartheta}^-_n$ as

$$\hat{\vartheta}_n = \hat{\vartheta}^-_n + K_n\left(g_n - H\hat{\vartheta}^-_n\right) \tag{15}$$

$$\rho C \frac{\vartheta^n_{i,j,k} - \vartheta^{n-1}_{i,j,k}}{\delta t} = \kappa \frac{\vartheta^{n-1}_{i-1,j,k} + \vartheta^{n-1}_{i+1,j,k} + \vartheta^{n-1}_{i,j-1,k} + \vartheta^{n-1}_{i,j+1,k} + \vartheta^{n-1}_{i,j,k-1} + \vartheta^{n-1}_{i,j,k+1} - 6\,\vartheta^{n-1}_{i,j,k}}{\delta^2} - \rho_b C_b w \vartheta^{n-1}_{i,j,k} + S_{i,j,k} u^{n-1} \tag{6}$$

where $g_n - H\hat{\vartheta}_n^-$ is called residual, which is zero in the absence of difference between the predicted and actual measurements. The $M \times L$ matrix K_n is the Kalman filter gain and is given by

$$K_n = P_n^- H^T \left(H P_n^- H^T + R \right)^{-1}. \tag{16}$$

The $M \times M$ matrix P_n^- is the *a priori* estimate error covariance. It is defined by the following equation:

$$P_n^- = \left\langle \left(\vartheta_n - \hat{\vartheta}_n^- \right) \left(\vartheta_n - \hat{\vartheta}_n^- \right)^T \right\rangle \tag{17}$$

where ^{T} denotes transposition. The Kalman filter cycles between the state update, which projects the current state estimate ahead in time, and the measurement update, which accounts for an actual measurement at that time. In the limit when the measurement noise covariance R approaches zero, the Kalman gain weights the residual more heavily and the actual measurement is more trusted in comparison with the predicted measurement, which is less trusted. The contrary is true in the limit when the *a priori* error covariance P_n^- approaches zero and the Kalman gain weights the residual less heavily, in which case, the predicted measurement is more trusted. Some useful equations are quoted in the Appendix.

V. Application to Temperature Monitoring During Brain Hypothermia

At a preliminary stage of the selective head cooling therapy, the knowledge of the achievable brain temperature is desirable, as well as its variation with time during treatment. There is the need, therefore, for noninvasive temperature measurement during treatments.

It seems worth investigating multifrequency radiometry potentiality for this measurement. The following procedure has been proposed in [11] for temperature retrieval. It is assumed that the temperature profile is a member of a class of profiles. The class is spanned by a linear combination of exponential functions whose space constants range in given intervals. The factors of the linear combination range in also given intervals. Space constants and factors are the unknowns of the inverse problem and are found exploiting radiometric data by a least square procedure. Suitable ranges are assumed from biophysical considerations as *a priori* information. The method can be simply implemented, but may provide wrong results in the case of mismatch between the *a priori* profile and "true" temperature. Instead, we can take advantage of the fact that the head is supposed to be monitored continuously during external cooling. The Kalman filtering is appropriate to perform this continuous monitoring and, in addition, has been proven to be robust against errors due to bad estimates of some parameters.

Since radiometric data for the baby-head treatment are not yet available, an inversion procedure can be only discussed basing on synthetic data, i.e., the data that are computed from (1) using realistic assumptions for the computation of temperature $T(\underline{r}, t) = T_0(\underline{r}) + \vartheta(\underline{r}, t)$ and weighting function $W_n(\underline{r'}) = W(\underline{r}_q, \underline{r'}, \delta B_p)$.

A few theoretical studies exist in the absence of measurements [21]. Since we are mainly interested in the microwave radiometry's performance, we neglect unnecessary morphological complications. Therefore, as in [26], the thermal model consists of a hemisphere Ω_H simulating the brain with surrounding bone and soft tissue. Two different boundaries are envisaged in the model. With reference to Fig. 1, B_1 is a hemispherical boundary between the upper head surface and either air (for $t < 0$) or a cooling fluid (for $t > 0$), while B_2 is a disk through which heat exchanges are localized with upper airways, spinal cord, and neck muscles. This thermal model was arranged in such a way to explain the cooling of a human brain during cold water (2 °C) near drowning. In this paper, conductive and convective exchanges with upper airways at B_2 have a minor effect besides also being a very complicated matter, therefore, an adiabatic $(h = 0)$ boundary condition is assumed on B_2. The temperature T_b of the blood perfusing the brain is assumed constant during a selective brain hypothermia treatment as a consequence of mild variations of the systemic temperature (see rectal-temperature diagrams in [15]). The diameter of Ω_H is assumed $2r = 10$ cm.

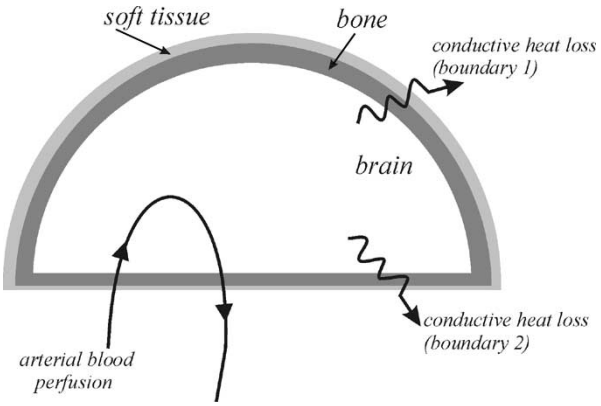

Fig. 1. Hemisphere model of head.

TABLE I
Thermal Parameters

	Soft Tissue	Bone	Brain	Blood
ρC [J/°C m^3]	$4.0 \cdot 10^6$	$2.3 \cdot 10^6$	$4.2 \cdot 10^6$	$4.2 \cdot 10^6$
κ [W/°C m]	0.47	0.75	0.49	
w_b [s^{-1}]	$3.3 \cdot 10^{-4}$	0	$8.4 \cdot 10^{-3}$	
M_0 [W/m^3]	$3.6 \cdot 10^2$	$3.7 \cdot 10^2$	$1.0 \cdot 10^4$	

The basal temperature T_0 is the steady-state solution of (3) for $T_b = 37$ °C, no external heat delivery and a boundary condition of type (4) on B_1 with external temperature $T_{env} = 29$ °C and $h = 8$ W°C^{-1}m^{-2}. The values of the other thermal parameters are listed in Table I (standard baby head). The transient solution $\vartheta(\underline{r}, t)$ is computed for a negative step of 19 °C, with $h = 400$ W°C^{-1}m^{-2}. Diagrams of ϑ are reported in Fig. 2 as a function of radial distance ς from the spherical boundary for various values of time.

The computation of the weighting functions requires the computation of the electromagnetic field inside the baby head for a realistic model of the radiometric antenna. We adopted the antenna already used in [11] (flanged rectangular waveguide—sizes 4×3 cm^2—fed by two orthogonal posts).

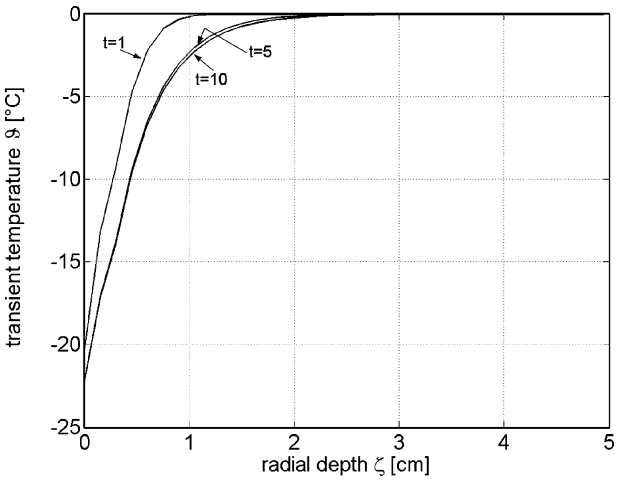

Fig. 2. Transient temperature ϑ versus radial distance ς from the scalp. Radiation for $t \geq 0$ onto a liquid at 10 °C surrounding the scalp. Time is in minutes.

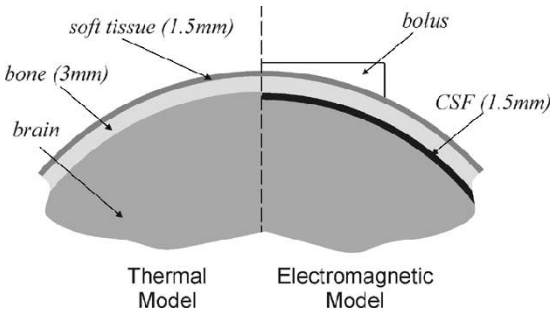

Fig. 3. Layered model of a hemispherical head.

TABLE II
ELECTROMAGNETIC PARAMETERS

		1.2GHz	3.0GHz
Bolus	ε_r	83.13	79.61
	σ [S/m]	0.497	2.965
Soft tissue	ε_r	30.59	29.04
	σ [S/m]	0.525	1.18
Bone	ε_r	8.01	7.97
	σ [S/m]	0.12	0.22
CSF	ε_r	64.83	62.85
	σ [S/m]	1.64	3.01
Brain	ε_r	53.83	51.22
	σ [S/m]	1.45	2.54

The presence of a bolus was assumed. The electromagnetic model of the neonatal head was a layered hemisphere, as in the thermal problem however, with two major remarks. First, the partition into cells for a finite-difference time-domain (FDTD) solution has been arranged in such a way as to become compatible with the thermal model. Second, the head layering includes materials (bolus and cerebral spinal fluid (CSF) layer), which are absent in the thermal model, but have some relevance in establishing the electromagnetic field pattern inside the head (Fig. 3). Indeed, computations accomplished with and without a CSF layer change by a few percents.

Two radiometric channels with center frequencies of 1.2 and 3.0 GHz have been considered. The tissue electrical parameters (Table II) have been taken as shown in [11]. The FDTD grid consists of cubic cells (size 0.15 cm) for 98 × 98 × 77 total

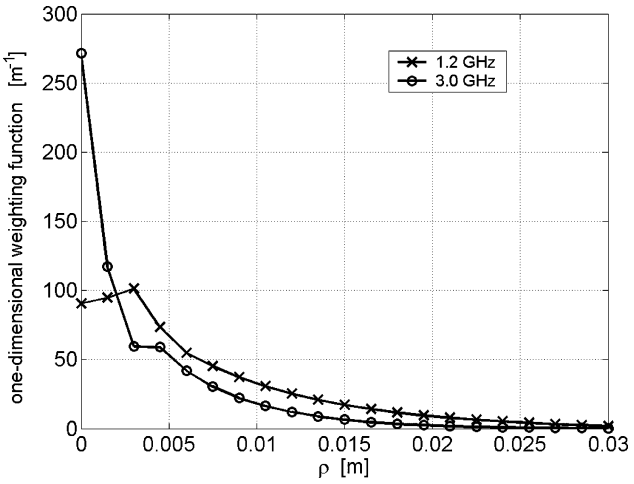

Fig. 4. Radiometric weighting functions versus radial distance for a layered hemispherical model of the head at two frequencies.

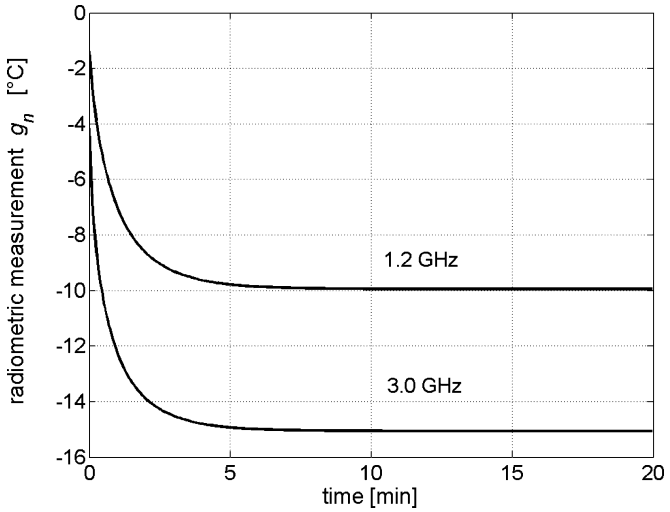

Fig. 5. Radiometric noiseless data g_n versus time for a layered hemispherical model of the standard baby head.

cells. Since the thermal model is one-dimensional in space, the weighting functions are averaged on concentric shell. The resulting one-dimensional weighting functions $W_n(\varsigma)$ are shown in Fig. 4. Their behaviors with depth are similar: a peak in the outer shells, then a monotonic decrease to negligible values at 3 cm from the surface.

Finally, the synthetic noiseless data can be obtained from (11); they are shown in Fig. 5 as functions of time. Radiometric data modeling is completed by addition of noise ν_n [see (12)]. We assume ν_n is a Gaussian white noise with standard deviation $\widetilde{\sigma}$ equal to the radiometric resolution (see Appendix) for both channels. Unless otherwise indicated, the radiometric resolution has been fixed to 0.04 °C, which is a practical value.

Temperature retrievals, which can be obtained when the same thermal model is used both as *a priori* information and to simulate radiometric data, show a temperature estimate that is indistinguishable from the "true" temperature. The agreement between the true temperature and an estimate is a trivial consequence of the coincidence of the thermal models used for both synthetic data generation and in a Kalman filter. In other words,

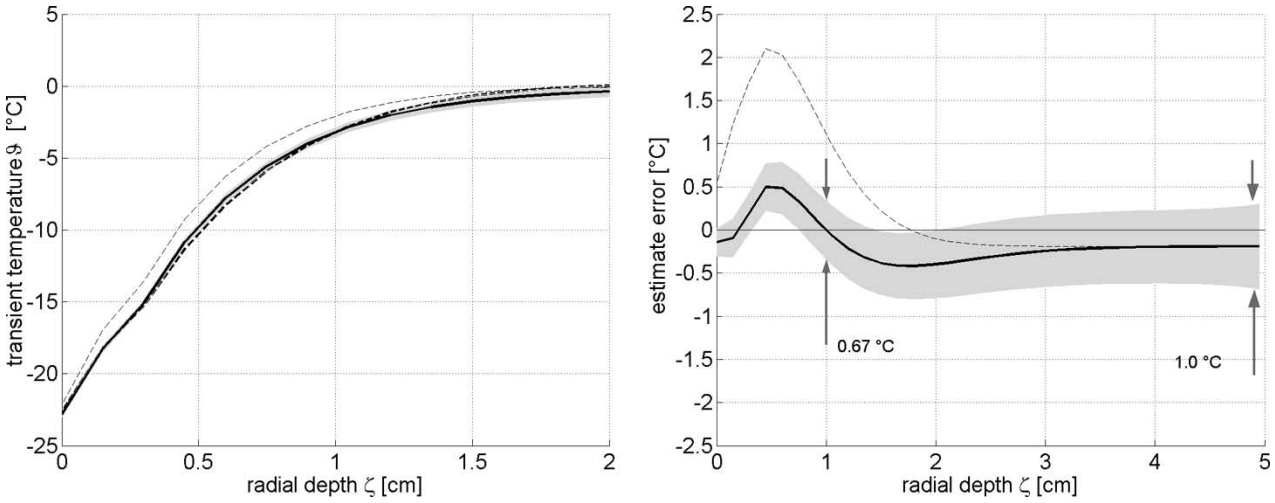

(a) (b)

Fig. 6. (a) Kalman filter temperature estimate $\hat{\vartheta}$ (solid curve), "true" temperature ϑ (thick dashed curve), "model" temperature (thin dashed curve) versus the distance from the scalp at $t = 4$ min. (b) Estimate error. $\tilde{\sigma} = 0.04$ °C. The perfusion rate in the baby head under measurement is lower (-50%) than in the standard baby head.

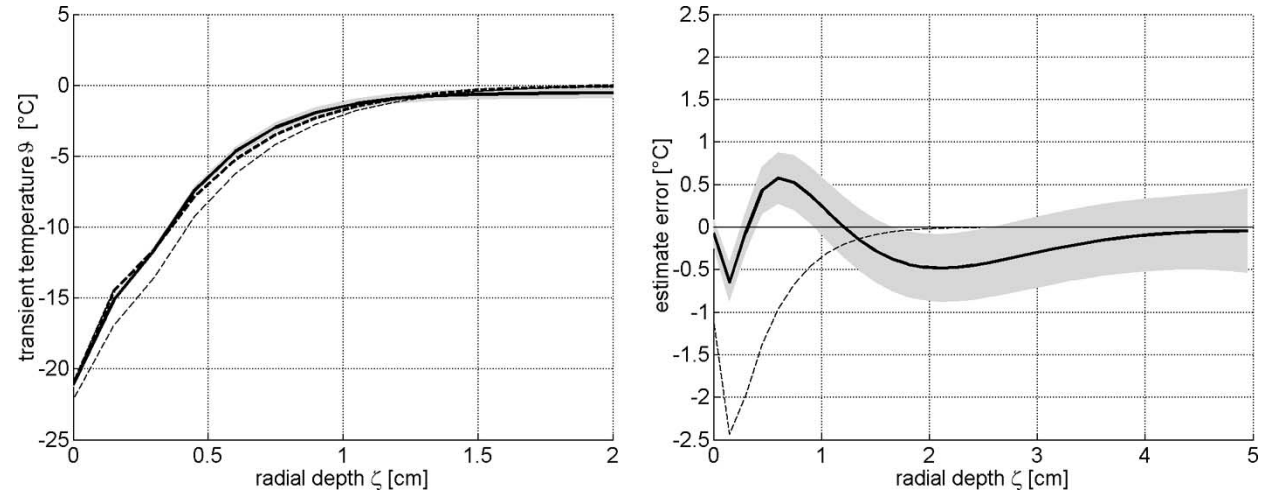

(a) (b)

Fig. 7. (a) Kalman filter temperature estimate $\hat{\vartheta}$ (solid curve), "true" temperature ϑ (thick dashed curve), "model" temperature (thin dashed curve) versus the distance from the scalp at $t = 4$ min. (b) Estimate error. $\tilde{\sigma} = 0.04$ °C. Thermal conductivity of the soft tissue in the baby under a measurement lower (-30%) than in the standard baby head.

if the *a priori* thermal model exactly reproduces the true temperature profile, measurements are not necessary.

In Figs. 6–8, the robustness of the inversion procedure against partially incorrect *a priori* information is checked. All the diagrams refer to $t = 4$ min. Grey bands show a $\pm 2\sigma$ confidence interval in the estimate, which is obtained from the *a posteriori* estimate error covariance P_n (see the Appendix). In Fig. 6, radiometric data were obtained by simulating a baby head with arterial blood perfusion rate lower (-50%) than the one assumed in the *a priori* model. In Fig. 7, a baby head with a thermal conductivity of the soft tissue lower (-30%) than the one assumed in the *a priori* model was simulated. Finally, in Fig. 8, the thermal conductivity of the brain of the baby head under simulated measurement was lower (-30%) than the one assumed in the *a priori* model.

The first two cases show a match between true and retrieved temperatures, which is, in a shell with depth up to approximately 2 cm, good if compared to the one obtained by using only the *a priori* model, i.e., without measurements. In the third case, the match becomes similar to the one obtained without measurements because the error in the *a priori* model was in the brain region, where the weighting functions rapidly vanish enabling the radiometric observation to become less effective.

It is worth evaluating the results of a different level of noise in the measurements. The noise standard deviation has been increased from 0.04 °C to 0.4 °C, thus simulating an integration time 100 times shorter. The same case of Fig. 6 has been considered, and some results are reported in Fig. 9. The peak value of the estimate error changes from 0.5 °C to approximately 1.2 °C, while the confidence interval slightly broadens. As expected, an increase in radiometric noise produces two adverse effects, i.e.: 1) a broadening of the confidence interval in the region sensed by the radiometer and 2) a growth of the estimate error in the same region.

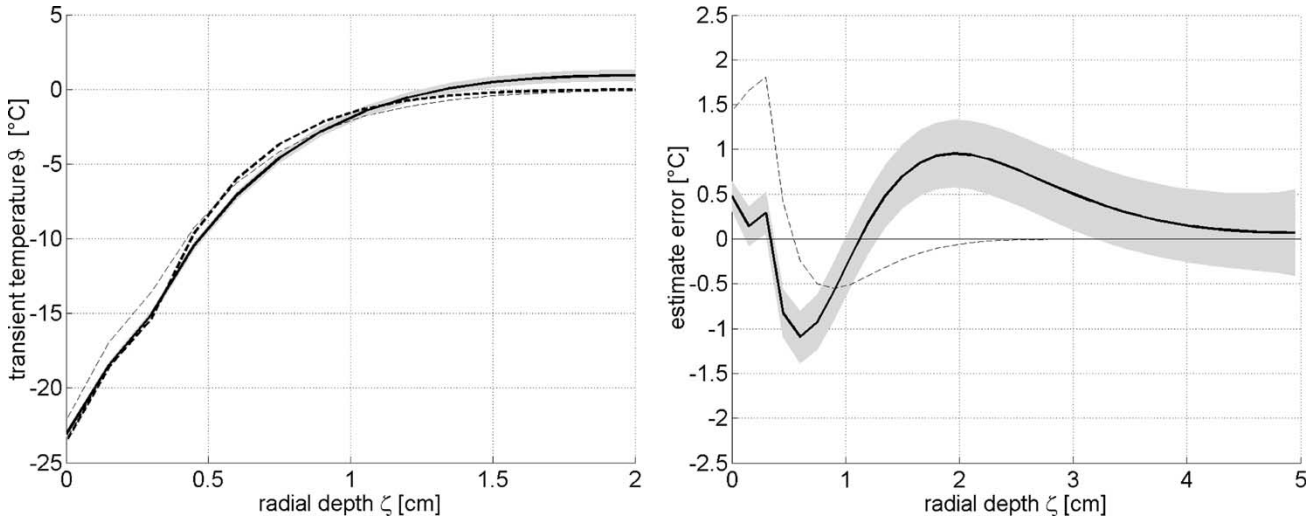

(a) (b)

Fig. 8. (a) Kalman filter temperature estimate $\hat{\vartheta}$ (solid curve), "true" temperature ϑ (thick dashed curve), "model" temperature (thin dashed curve) versus distance from the scalp at $t = 4$ min. (b) Estimate error. $\widetilde{\sigma} = 0.04$ °C. Thermal conductivity of the brain in the baby under a measurement lower (-30%) than in the standard baby head.

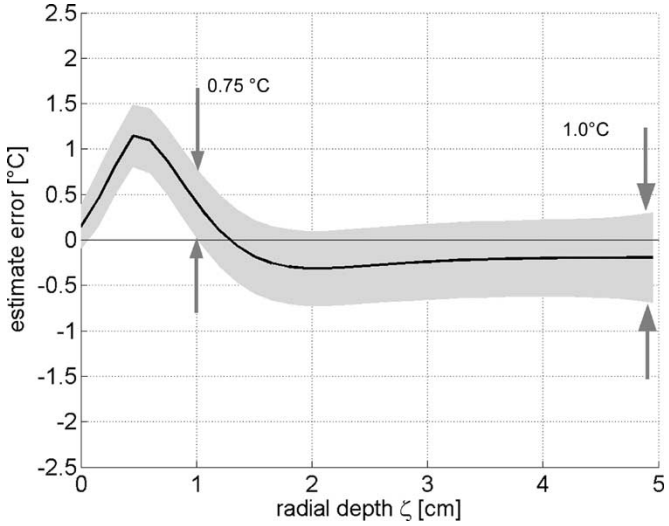

Fig. 9. Estimate error and confidence interval for the same case of Fig. 6, but for $\widetilde{\sigma} = 0.4$ °C.

VI. Conclusions

Multifrequency microwave radiometry has been considered for the measurement of temperature during therapeutic treatments with heat delivery or subtraction. A thermal model has been arranged from Pennes' equation and cast as a discrete-time controlled statistical process. The measurement equation has been obtained from the radiometer integral equation. Temperature is estimated by Kalman filtering of noisy radiometric data. A numerical analysis has been performed simulating a two-channel system monitoring of a hypothermia treatment in a baby head. The results show that the radiometric measurements can compensate for uncertainties in the model. The sensing depth is limited to approximately 2 cm from the scalp by the relevant conductive properties of the brain and by the CSF barrier in the provided example. However, the two-channel radiometer is able to give an accurate and robust estimate of temperature in the 1.5 cm outer layer of the brain.

Appendix

The Kalman filter equations for the process are

$$\hat{\vartheta}_n^- = A\hat{\vartheta}_{n-1} + Bu_{n-1} \tag{A1}$$

$$P_n^- = AP_{n-1}A^T + Q \tag{A2}$$

which, respectively, update the *a priori* state estimate and *a priori* estimate error covariance (17). The *a posteriori* estimate is updated by (15) and (16) taking measurements into account. The *a posteriori* estimate error covariance in (A2) is defined as

$$P_n = \left\langle \left(\vartheta_n - \hat{\vartheta}_n\right)\left(\vartheta_n - \hat{\vartheta}_n\right)^T \right\rangle. \tag{A3}$$

It is computed from

$$P_n = (I - K_n H)P_n^- \tag{A4}$$

where I is the identity matrix.

In the above numerical analysis, the filter is initialized with $R = \widetilde{\sigma}^2 I$ and $\widetilde{\sigma} = 0.04$ °C. In practice, we assume that the various measurements are affected with noncorrelated noise of identical statistical properties. The parameter $\widetilde{\sigma}$ is called the radiometric resolution of a radiometric channel. It is related to the equipment in use and to the integration time τ, already introduced above in the main text. For an ideal balanced Dicke radiometer [27], the radiometric resolution is

$$\widetilde{\sigma} = \frac{2(T_a + T_{\mathrm{rec}})}{\sqrt{\delta B \tau}} \tag{A5}$$

where T_{rec} is the receiver input noise-equivalent temperature, δB is the bandwidth (in hertz), and τ is in seconds. T_a and T_{rec} are in kelvin. It is worth mentioning that τ has to be $\leq$ the time interval between two consecutive measurements, which, in turn, is the time step δt of the discrete-time process.

On the basis of heuristic reasoning, the state noise covariance matrix Q has been taken as $Q = \sigma_x^2 I$ and $\sigma_x = 0.1$ °C, and then

the estimate error covariance matrices P_n^- and P_n are computed for increasing n with (A2) and (A3).

REFERENCES

[1] E. Schanda, *Passive Microwave Sensing in Remote Sensing for Environmental Sciences*, E. Schanda, Ed. Berlin, Germany: Springer-Verlag, 1976.

[2] B. Enander and G. Larson, "Microwave radiometric measurements of the temperature inside a body," *Electron. Lett.*, vol. 10, pp. 317–318, 1974.

[3] J. Edrich, "Centimeter and millimeter wave thermography. A survey on tumor detection," *J. Microwave Power*, vol. 14, pp. 95–104, 1979.

[4] P. C. Myers, N. L. Sadowsky, and A. H. Barrett, "Microwave thermography: Princples, methods and clinical applications," *J. Microwave Power*, vol. 14, pp. 105–115, 1979.

[5] D. D. N'Guyen, A. Mamouni, Y. Leroy, and E. Constant, "Simultaneous microwave local heating and microwave thermography: Possible clinical applications," *J. Microwave Power*, vol. 14, pp. 135–137, 1979.

[6] F. Bardati and D. Solimini, "Radiometric sensing of biological layered media," *Radio Sci.*, vol. 18, pp. 1393–1401, 1983.

[7] D. V. Land and V. J. Brown, "Subcutaneous temperature measurement by microwave radiometry," in *Proc. 17th Eur. Microwave Conf.*, Rome, Italy, 1987, pp. 896–900.

[8] Y. Hamamura, S. Mizushina, and T. Sugiura, "Non-invasive measurement of temperature-versus-depth profile in biological systems using a multiple-frequency-band microwave radiometer system," *Automedica*, vol. 8, pp. 213–216, 1987.

[9] L. Dubois, J. Pribetich, J. J. Fabre, M. Chivé, and Y. Moschetto, "Non-invasive microwave multifrequency radiometry used in microwave hyperthermia for bidimensional reconstruction of temperature patterns," *Int. J. Hyperthermia*, vol. 9, pp. 415–431, 1993.

[10] K. L. Carr, A. M. El-Mahdi, and J. Schaeffer, "Passive microwave thermography coupled with microwave heating to enhance early detection of cancer," *Microwave J.*, vol. 25, pp. 135–136, 1982.

[11] K. Maruyma, S. Mizushina, T. Sugiura, G. M. J. Van Leeuwen, J. W. Hand, G. Marrocco, F. Bardati, A. D. Edwards, D. Azzopardi, and D. Land, "Feasibility of noninvasive measurement of deep brain temperature in new-born infants by multifrequency microwave radiometry," *IEEE Trans. Microwave Theory Tech.*, vol. 48, pp. 2141–2147, Dec. 2000.

[12] F. Bardati, M. Bertero, M. Mongiardo, and D. Solimini, "Singular system analysis of the inversion of microwave radiometric data: Applications to biological temperature retrieval," *Inverse Problems*, vol. 3, pp. 347–369, 1987.

[13] J. Tooley, S. Satas, R. Eagle, I. A. Silver, and M. Thoresen, "Significant selective head cooling can be maintained long-term after global hypoxia ischemia in newborn piglets," *Pediatrics*, vol. 109, pp. 643–649, Apr. 2002.

[14] R. A. Kilani, "The safety and practicality of selective head cooling in asphyxiated human newborn infants, a retrospective study," *Lebanese Med. J.*, vol. 50, pp. 17–22, 2002.

[15] O. Iwata, S. Iwata, M. Tamura, T. Nakamura, M. Sugiura, and Y. Ogiso, "Brain temperature in newborn piglets under selective head cooling with minimal systemic hypothermia," *Pediatrics Int.*, vol. 45, pp. 163–168, Apr. 2003.

[16] A. J. Gunn, P. D. Gluckman, and T. R. Gunn, "Selective head cooling in newborn infants after perinatal asphyxia: A safety study," *Pediatrics*, vol. 102, pp. 885–892, 1998.

[17] D. Azzopardi, F. M. Cowan, N. J. Robertson, and A. D. Edwards, "Mild whole body hypothermia following birth asphyxia," *Pediatric Res.*, vol. 45, p. 308, 1999.

[18] F. Bardati and D. Solimini, "On the emissivity of layered materials," *IEEE Trans. Geosci. Electron.*, vol. GE-22, pp. 374–376, July 1984.

[19] F. Bardati, V. J. Brown, and P. Tognolatti, "Temperature reconstructions in a dielectric cylinder by multi-frequency microwave radiometry," *J. Electromagn. Wave Applicat.*, vol. 7, pp. 1549–1571, 1993.

[20] H. H. Pennes, "Analysis of tissue and arterial blood temperatures in the resting human forearm," *J. Appl. Physiol.*, vol. 1, pp. 93–122, 1948.

[21] G. M. J. Van Leeuwen, J. W. Hand, J. J. W. Lagendijk, D. Azzopardi, and A. D. Edwards, "Numerical modeling of temperature distributions within the neonatal head," *Pediatric Res.*, vol. 48, pp. 351–356, 2000.

[22] A. R. Mitchell and D. F. Griffiths, *The Finite Difference Method in Partial Differential Equations*. Chichester, U.K.: Wiley, 1980.

[23] C. De Wagter, "Optimization of simulated two-dimensional temperature distributions induced by multiple electromagnetic applicators," *IEEE Trans. Microwave Theory Tech.*, vol. MTT-34, pp. 589–596, May 1986.

[24] A. Gelb, *Applied Optimal Estimation*. Cambridge, MA: MIT Press, 1974.

[25] G. Welch and G. Bishop, "An introduction to the Kalman filter," Dept. Comput. Sci., Univ. North Carolina at Chapel Hill, Chapel Hill, NC, Tech. Rep. TR 95-041, May 23, 2003.

[26] X. Xu, P. Tikuisis, and G. Giesbrecht, "A mathematical model for human brain cooling during cold-water near drowning," *J. Appl. Physiol.*, vol. 86, pp. 265–272, 1999.

[27] F. Ulaby, R. Moore, and A. Fung, *Microwave Remote Sensing—Active and Passive*. Norwood, MA: Artech House, 1981, vol. I.

Fernando Bardati received the Laurea degree in electronic engineering and Libero Docente degree of microwaves from the Università degli Studi di Roma "La Sapienza," Rome, Italy, in 1965 and 1971, respectively.

He is currently is Full Professor of electromagnetic fields of the Faculty of Engineering, Università degli Studi di Roma "Tor Vergata." His research interests are electromagnetic propagation in anisotropic media, numerical methods for electromagnetic field computation, antenna synthesis, bioelectromagnetic interactions for safety, and therapeutic and diagnostic applications.

Prof. Bardati is a member of several professional societies, review boards, and governmental commissions for applied research.

Gaetano Marrocco (S'96–M'98) received the Laurea degree in electronic engineering and Ph.D. degree in applied electromagnetics from the Università degli Studi dell' Aquila, L'Aquila, Italy, in 1994 and 1998, respectively.

Since 1997, he has been a Researcher with the Università degli Studi di Roma "Tor Vergata," Rome, Italy, where he currently teaches antenna design. In the summer of 1994, he was a post-graduate student with the University of Illinois. In the autumn of 1999, he was a Visiting Researcher with Imperial College, London, U.K. His research is mainly directed to the development of numerical methods and signal-processing techniques for the time-domain modeling of complex electromagnetic structures in the context of biological and aerospace applications. He has been involved in several space, avionic and naval programs of the European Space Agency, North-American Treaty Organization (NATO), Italian Space Agency and Italian Navy.

Piero Tognolatti (M'83) received the Laurea degree in electronic engineering from the Università degli Studi di Roma "La Sapienza," Rome, Italy, in 1981.

From 1982 to 1984, he was with the Research and Development Division, Telespazio S.p.A. (the Italian satellite communication company). From 1984 to 1992, he was a Researcher with the Università degli Studi di Roma "Tor Vergata," where he was involved with electromagnetic fields. In 1992, he joined the Università degli Studi dell' Aquila, l'Aquila, Italy, as an Associate Professor. Since 2000, he has been a Full Professor of microwaves at the Università degli Studi dell' Aquila. His main scientific interests are medical application of microwaves, antenna and passive microwave circuit design, numerical techniques, and electromagnetic compatibility.